

It's not a Lottery, it's a Race: Understanding How Gradient Descent Adapts the Network's Capacity to the Task

Hannah Pinson¹

Abstract

Our theoretical understanding of neural networks is lagging behind their empirical success. One of the important unexplained phenomena is why and how, during the process of training with gradient descent, the theoretical capacity of neural networks is reduced to an effective capacity that fits the task. We here investigate the mechanism by which gradient descent achieves this through analyzing the learning dynamics at the level of individual neurons in single hidden layer ReLU networks. We identify three dynamical principles -mutual alignment, unlocking and racing- that together explain why we can often successfully reduce capacity after training through the merging of equivalent neurons or the pruning of low norm weights. We specifically explain the mechanism behind the lottery ticket conjecture, or why the specific, beneficial initial conditions of some neurons lead them to obtain higher weight norms.

1. Introduction

Modern neural networks are very large or even overparameterized: they have more parameters than input samples. After training, they can often be pruned or compressed (Zhu & Gupta, 2017; Frantar & Alistarh, 2023; Hoeferl et al., 2021; Cheng et al., 2024), indicating that the final function they implement can actually be represented using (far) fewer parameters. This excess of parameters leads to higher computational costs. Still, it is found that overparameterized networks generalize better, a phenomenon explained by the implicit bias of gradient descent (Neyshabur et al., 2015; Du & Lee, 2018; Nacson et al., 2019; Ji & Telgarsky, 2020; Advani et al., 2020).

A closely related concept is that of lottery tickets (for a survey, see (Liu et al., 2024)). In the original paper on lottery

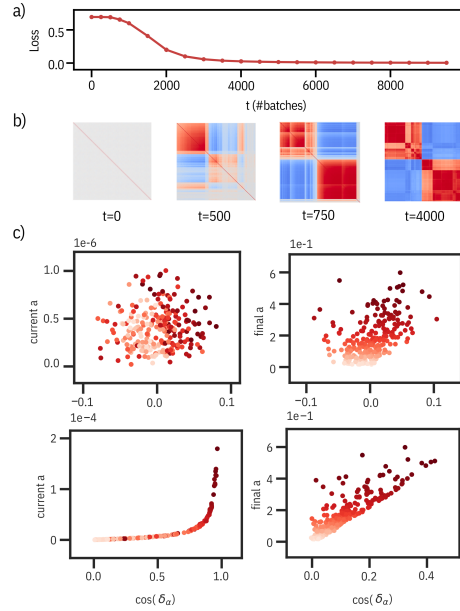


Figure 1. Experimental results for a binary classification task based on the CIFAR10 dataset. a) Evolution of the training loss. b) Cosine similarity matrices between the total parameter vectors of individual neurons at different timesteps during training. Over time, individual neurons start to (mutually) align to shared target directions. (Neuron ordering is different from matrix to matrix). c) Illustration of how well the angular distance δ_α of the incoming weight vector of a neuron α to its target direction early in training predicts the neuron's final total norm, denoted $a_\alpha = \|\vec{w}_\alpha^{(2)}\|/\|\vec{w}_\alpha^{(1)}\|$. Upper row shows the results at initialization ($t=0$), the lower row at a timepoint early in training ($t=500$), before the loss drops. In the left column, we plot the current value a_α in function of $\cos(\delta_\alpha)$. In the right column, we plot the final value for a_α in function of the same values $\cos(\delta_\alpha)$, i.e., the values of $\cos(\delta_\alpha)$ at $t=0$ and $t=500$. In both columns, neurons have a darker color if they have a higher final norm. This shows that we can, to a large degree, predict which neurons will obtain a higher final norm from looking at the angular distance to their target direction at initialization (upper row). We argue that this arises because, in the early phase of learning, neurons that arrive earlier at their target direction (because they were oriented favorably to start with) grow exponentially faster in norm. This can be seen in the lower row, and is explained in our theoretical results.

¹Data and AI cluster / EAISI , Eindhoven University of Technology, The Netherlands. Correspondence to: Hannah Pinson <h.pinson@tue.nl>.

which, when trained in isolation, reaches a similar performance as the full network. They showed such networks can be discovered *after* (some) training based on the pruning of weights with lower norms. The exact initialization values are key: the discovered subnetwork needs to be trained from its original initial conditions to reach a similar performance as the full network. The name for these types of subnetworks, ‘lottery tickets’, reflects their lucky initialization. From this point of view, training overparameterized networks with gradient descent can be seen as a mechanism to select optimally initialized subnetworks through the amplification of their parameter norms (Morcos et al., 2019). The existence of the subnetworks at initialization is the so-called *lottery ticket hypothesis*. The idea that gradient descent selects these subnetworks is called the *lottery ticket conjecture* (Frankle & Carbin, 2019).

It has been shown that lottery tickets can be found in a wide range of architectures (Liu et al., 2024), including transformers and LLMs (Brix et al., 2020; Behnke & Heafield, 2020). There is also a proof of the lottery ticket hypothesis itself (Malach et al., 2020). In terms of the conjecture, i.e., how gradient descent amplifies the norms of the lottery tickets, there are some limited results: it is found that lottery tickets can be discovered through pruning already in the early stages of training (Frankle et al., 2020b), that the signs of the initializations matter more than the values (Zhou et al., 2019), and that the same lottery tickets can be used for similar datasets (Morcos et al., 2019), indicating a strong dependence of a lottery ticket on the (general) features of the dataset it was trained on. In (Paul et al., 2022; Frankle et al., 2020a), the authors link the success of (iterative) pruning used to discover lottery tickets to the robustness of gradient descent and linear mode connectivity. However, both the exact nature of the beneficial initial conditions, as well as how exactly gradient descent leads to lottery ticket obtaining a larger norm compared to other parts of the network, remains an open question.

In this paper we analyze the learning dynamics, i.e., the evolution of the parameters under the influence of gradient descent, of individual neurons in single hidden layer ReLU networks for binary classification tasks, and this in the feature learning regime (Woodworth et al., 2020).

Our contributions are the following:

- from a mathematical analysis of the dynamics of gradient descent, we identify three important dynamical principles (mutual alignment, unlocking and racing) that guide the general evolution of the parameters of the individual neurons,
- we explain how these dynamical principles in our specific setting can give rise to a reduction in effective capacity in terms of equivalent neurons that can be merged,
- we explain how these same dynamical principles explain the nature of the beneficial initial conditions of

lottery tickets,

- we reveal how these principles lead to corresponding neurons obtaining a higher norm for their associated parameters,
- and we discuss to what degree we can really predict lottery tickets at initialization and early in training.

The notion of (mutual) alignment we here discuss is not novel: it has been shown before that, under the influence of gradient descent, weight vectors of networks trained in the rich regime tend to align to a (smaller) set of target directions related to the dataset (Soudry et al., 2018; Gur-Ari et al., 2018; Atanasov et al., 2022). These directions can be exactly or approximately calculated for simplified settings, such as linear networks, isotropic datasets or single neurons (Atanasov et al., 2022; Saxe et al., 2022; Refinetti et al., 2023). Alignment is directly related to a reduction in effective capacity (Baratin et al., 2021; Kopitkov & Indelman, 2020; Paccolat et al., 2021), as it reduces the dimension of the feature space implemented by the weights. In (Atanasov et al., 2022), the authors introduce the notion of ‘silent alignment’: the fact that this alignment often takes place early in training, *before* the loss considerably drops, yielding a clear separation in time between changes in weight vector directions and changes in their norm (and subsequently in the loss).

The crucial and new observation we here make is that there is no complete decoupling between changes in direction and changes in norm: we find, in fact, that the growth in norm exponentially depends on the angular distance to the (current) target direction. This creates a ‘winner-takes-all’ dynamic (Fukai & Tanaka, 1997): neurons which are initialized closer to their target directions can grow more quickly in norm. Optimally aligned neurons that increase in norm, reduce the loss and solve the task. Thus the neurons that arrive earlier strongly reduce the loss and gradients, and therefore they inhibit the development of other neurons. In general, a few neurons which have the ‘luck’ to be initialized close to their target direction, thus obtain a higher norm and contribute more to the solution of the task; at the same time, other, less important neurons do not grow significantly in norm. The latter neurons can subsequently be pruned. In short, we thus find that gradient descent implicitly selects lottery tickets in a process more akin to dynamical race than a static lottery.

2. Related Work

Our analysis is closely related to the study of gradient descent dynamics for linear networks (Saxe et al., 2019; Tarnouni et al., 2021; J Dominé et al., 2023; Pinson et al., 2023; Gidel et al., 2019) and extensions to nonlinear networks in simplified settings (Tachet et al., 2020; Refinetti et al., 2023; Jarvis et al., 2025). We here use a ReLU network including a softmax function and a cross-entropy loss, which makes

our setting closer to networks used in practice. But more importantly, these works assume completely silent alignment, and/or do not focus on the dynamics of individual neurons within a network. Another line of related work relates iterative pruning based on magnitudes to the discovery of inductive biases, more specifically, the discovery of local receptive fields in fully connected networks (Pellegrini & Biroli, 2022; Redman et al., 2025). Lastly, some works study the prediction of lottery tickets at initialization or early in training. In (Frankle et al., 2020a;b), the authors show experimentally that lottery tickets are largely determined early in training, and multiple experimental methods exist to perform pruning at those early stages (Lee et al., 2019; Wang et al., 2020). Our work provides the theoretical basis to understand the success of those methods.

3. Preliminaries and Notation

3.1. Single Hidden Layer ReLU Networks

Let $\{(\vec{x}^s, \vec{y}^s)\}_{s=1}^N \subseteq \mathbb{R}^N \times \{\begin{bmatrix} 1 \\ 0 \end{bmatrix}, \begin{bmatrix} 0 \\ 1 \end{bmatrix}\}$ be a binary classification dataset. We consider the single hidden layer neural network with d neurons in the hidden layer:

$$\vec{h}^s = \text{ReLU}(W^{(1)}\vec{x}^s + \vec{b}^{(1)}) \quad (1)$$

$$\vec{z}^s = W^{(2)}\vec{h}^s + \vec{b}^{(2)} \quad (2)$$

$$\hat{\vec{y}}^s = \text{softmax}(\vec{z}^s) \quad (3)$$

trained with gradient descent for a classification task using a binary cross-entropy loss (in our setup with two output classes): $L^s = -\sum_{i=0}^1 \vec{y}_i^s \log(\hat{y}_i^s)$ here given for a single sample s . We denote the vector of incoming weights to a neuron indexed by α as $\vec{w}_\alpha^{(1)} = W_{\alpha,:}^{(1)}$ and the 1×2 (row) vector of its outgoing weights as $\vec{w}_\alpha^{(2)} = \mathbf{W}_{:, \alpha}^{(2)}$. The d_{input} angles of $\vec{w}_\alpha^{(1)}$ in a (hyper)spherical coordinate system are denoted $\theta_{\alpha,i}$ with $i \in 0, \dots, d_{\text{input}}$ and d_{input} the dimension of the input. The angle of $\vec{w}_\alpha^{(2)}$ is denoted ϕ_α . We furthermore define a set of vectors $\vec{\Delta y}^s$ for each sample s at each point of training, where $\vec{\Delta y}^s = \vec{y}^s - \hat{\vec{y}}^s$, with corresponding angle $\phi_{\vec{\Delta y}^s}$.

3.2. ReLUs as gates and effective datasets

ReLU activation functions effectively act as gates: positive values are passed without modification, and negative values result in zero. At any point during training, we can determine what we call the ‘gating vector’ \vec{g}_α of a neuron α : \vec{g}_α is a vector of dimension $d_{\text{input}} \times 1$ with values either 0 or 1, such that g_α^s represents whether the incoming sample is passed on ($g_\alpha^s = 1$) or blocked ($g_\alpha^s = 0$) by the ReLU activation of neuron α . From this point of view, each neurons only ‘sees’ an effective dataset given by the samples that pass its gates, as the other samples do not contribute to its activations or gradients. The total task/dataset can thus be seen as

an overlapping collection of effective tasks/datasets, and if we only consider its effective samples, each neuron acts as a linear function. This principle has been used to describe the dynamics of ReLU networks with MSE loss and complete silent alignment through approximating the ReLUs as fixed gates (Saxe et al., 2022; Jarvis et al., 2025). But in general \vec{g}_α changes over training time, i.e., $\vec{g}_\alpha = \vec{g}_\alpha(t)$. This makes analyzing the learning dynamics of the network overall very challenging. In our analysis, we will argue why during some intervals during training, we can consider the gating to be fixed for a subset of neurons, and why this is sufficient to describe the dynamical principles we are interested in. In terms of notation, we will use $\langle \cdot \rangle$ to denote an average over all samples that pass the ReLU gate of the given neuron, i.e., the average over the effective dataset of a given parameter p_α : $\langle p_\alpha \rangle = \frac{1}{N} \sum_s^N g_\alpha^s p_\alpha^s = \frac{1}{N} \sum_s^{N^e} p_\alpha^s$, with N^e the number of effective samples. We will use the notation $\langle p_\alpha \rangle_{C_1}$ to denote an average over all *effective* samples of class 1, and $\langle p_\alpha \rangle_{C_2}$ for an average over *effective* samples of class 2. N_1^e and N_2^e denote the number of effective samples of class 1 and 2, respectively.

3.3. Gradient flow

When studying learning dynamics, it is customary to consider gradient flow, the continuous approximation to the discrete updates of gradient descent (Saxe et al., 2019). When the learning rate is low, the parameters of the network change only slightly with each new sample provided to the network. Under these conditions, we can approximate the change in a parameter over a set of samples through using the average of the gradients obtained over this set of samples $\Delta p \approx -\lambda N \langle \frac{\partial L^s}{\partial p} \rangle$, with λ the learning rate and N the number of samples/updates. We can then consider the continuous time limit, and obtain for each parameter the differential equation $\frac{\partial p}{\partial t} = -\lambda \langle \frac{\partial L^s}{\partial p} \rangle$.

4. Mathematical Theory

4.1. Equations of Gradient Descent

We here first write out the gradients in full *for a fixed gating vector \vec{g}_α* :

$$\langle \frac{\partial L^s}{\partial \phi_\alpha} \rangle = -\|\vec{w}_\alpha^{(2)}\| \langle h_\alpha^s \|\vec{\Delta y}^s\| \sin(\phi_{\vec{\Delta y}^s} - \phi_\alpha) \rangle \quad (4)$$

$$\langle \frac{\partial L^s}{\partial \|\vec{w}_\alpha^{(2)}\|} \rangle = -\langle h_\alpha^s \|\vec{\Delta y}^s\| \cos(\phi_{\vec{\Delta y}^s} - \phi_\alpha) \rangle \quad (5)$$

$$\langle \frac{\partial L^s}{\partial (\theta_{\alpha,i})} \rangle = -\|\vec{w}_\alpha^{(2)}\| \|\vec{w}_\alpha^{(1)}\| \|\langle \vec{\gamma}_\alpha^s \rangle\| \sin(\theta_{\langle \vec{\gamma}_\alpha^s \rangle, i} - \theta_{\alpha,i}) \quad (6)$$

$$\langle \frac{\partial L^s}{\partial \|\vec{w}_\alpha^{(1)}\|} \rangle = -\|\vec{w}_\alpha^{(2)}\| \|\langle \vec{\gamma}_\alpha^s \rangle\| \cos(\theta_{\langle \vec{\gamma}_\alpha^s \rangle, i} - \theta_{\alpha,i}) \quad (7)$$

$$\langle \frac{\partial L^s}{\partial b_\alpha} \rangle = -\|\vec{w}_\alpha^{(2)}\| \langle \|\vec{\Delta y}^s\| \cos(\phi_{\vec{\Delta y}^s} - \phi_\alpha) \rangle \quad (8)$$

in a form that will allow us to more easily derive the dy-

namical principles we are interested in. Note that the fixed gating vector is reflected in the averages, which are taken over the effective dataset. Details can be found in appendix B. We here used the vector:

$$\langle \vec{\gamma}_\alpha^s \rangle = \frac{1}{N} \sum_s^N g_\alpha^s \cos(\phi_{\Delta y^s} - \phi_\alpha) \|\Delta \vec{y}^s\| \vec{x}^s \quad (9)$$

which, as we will show, plays a central role in the dynamics. This vector depends on training time through $\vec{\gamma}_\alpha^s = \vec{\gamma}_\alpha^s(t)$ and $\Delta \vec{y}^s = \Delta \vec{y}^s(t)$.

4.2. (Mutual) Alignment

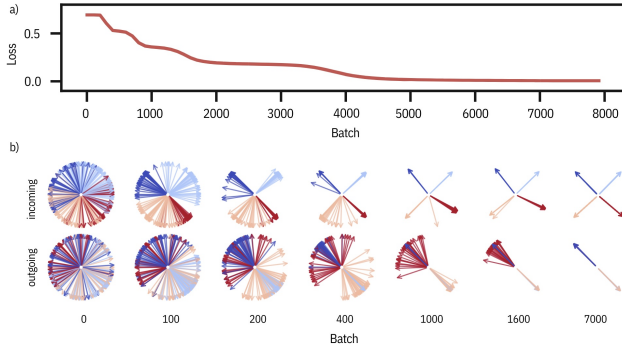


Figure 2. Visualization of alignment for a simple dataset XOR-like dataset (illustrated in fig. 9), but where the centroids of the 4 different clusters have 4 different norms. a) Training loss, showing 4 drops in loss. b) Visualization of the directions of the vectors of incoming weights (upper row) and vectors of outgoing weights (lower row) of each of the neurons during training. Vectors are colored according to which final direction they align to. The alignment process takes place at 4 different speeds (light blue is the fastest, red the slowest), corresponding to 4 different subsystems of neurons. For this simple dataset, the vectors remain aligned after the initial drops in the loss.

We here revisit the phenomenon of silent alignment, and characterise the directions the neurons in our setup converge to. In fig. 2, we show how the directions of the incoming and outgoing weight vectors of a network trained on a XOR-like dataset change over time. As we start from random initial conditions, the vectors initially point in random directions; however, just before each loss drop, the corresponding vectors finish their mutual alignment to a set of task-relevant directions. In the case of this simple XOR-like dataset, the weight vectors remain aligned to these directions.

To explain this and more complex behavior, we consider that, for a given, *fixed* gating vector and a given neuron, the target directions (for its incoming and outgoing weights) are given by $\frac{\partial \phi_\alpha^*}{\partial t} = -\lambda \langle \frac{\partial L^s}{\partial \phi_\alpha^*} \rangle = 0$ (cfr. sec. 3.3 and eq. 4) and $\frac{\partial \theta_{\alpha,i}^*}{\partial t} = -\lambda \langle \frac{\partial L^s}{\partial \theta_{\alpha,i}^*} \rangle = 0$ (cfr. sec. 3.3 and eq. 6). Let's start with the direction of the outgoing weights, $\frac{\partial \phi_\alpha^*}{\partial t} = 0$. We first need to note that $\phi_{\Delta y^s}$ is always $\phi_{\Delta y^s} = \frac{7\pi}{4} + n2\pi$ for samples of class 1, and $\phi_{\Delta y^s} = \frac{3\pi}{4} + n2\pi$ for samples

of class 2 (details, see appendix C). If ϕ_α becomes equal to one of these values, the factor $\sin(\phi_{\Delta y^s} - \phi_\alpha)$ in eq. 4 is zero for all samples s. Through a computation of the second derivative, we can determine which of these values ϕ_α will converge to. We obtain:

Theorem 4.1. *For a fixed gating pattern \vec{g}_α , the target direction for the outgoing weight vector ϕ_α^* is given by:*

$$\phi_\alpha^* = \phi_\alpha^{*1} \equiv \frac{7\pi}{4} + n2\pi \text{ when } \vec{w}_\alpha^{(1)} \vec{\xi}_1 > \vec{w}_\alpha^{(1)} \vec{\xi}_2 \quad (10)$$

$$\phi_\alpha^* = \phi_\alpha^{*2} \equiv \frac{3\pi}{4} + n2\pi \text{ when } \vec{w}_\alpha^{(1)} \vec{\xi}_1 < \vec{w}_\alpha^{(1)} \vec{\xi}_2 \quad (11)$$

$$\vec{\xi}_1 \equiv N_1^e \langle \|\Delta y^s\| \vec{x}^s \rangle_{C_1}, \vec{\xi}_2 \equiv N_2^e \langle \|\Delta y^s\| \vec{x}^s \rangle_{C_2}. \quad (12)$$

These are exactly the angles obtained in the simple XOR-like experiment, see fig. 2b, bottom row. In fact, the set of angles $\{\phi_\alpha^{*1}, \phi_\alpha^{*2}\}$ is the same for any dataset, gating pattern and neuron, but the effective dataset and initial orientation of the incoming weights of the neuron influence which of those two angles the outgoing weights of the neuron will converge to. Considering $\|\Delta y^s\| \approx \frac{\sqrt{2}}{2}$ for all samples at the beginning of training (as $\vec{y}^s \approx [0.5 \ 0.5]$), we can see that the outgoing weights of a neuron will have ϕ_α^{*1} as a target direction as long as its incoming weight vector is closer oriented to the sum of the effective samples of class one than to the sum of the effective samples of class two (and vice versa), $\vec{w}_\alpha^{(1)} N_1^e \langle \vec{x}^s \rangle_{C_1} > \vec{w}_\alpha^{(1)} N_2^e \langle \vec{x}^s \rangle_{C_2}$. To gain insight in this, it's important to realise that when $\phi_\alpha = \phi_\alpha^{*1}$, this implies $\vec{w}_\alpha^{(2)} = k[-1]$ for a positive scalar k , meaning the neuron always increases the value of output node 1 and decreases the value of node 2 (hence the notation ϕ_α^{*1}) for all samples that pass its gate, irrespective of their class. On the other hand, $\phi_\alpha = \phi_\alpha^{*2}$ implies $\vec{w}_\alpha^{(2)} = k[-1]$, thus a neuron with outgoing weights with this direction always increases the value of output node 2. In short, if the incoming weight vector of a neuron is oriented to receive more 'signal' of a given class, it will orient its outgoing weights to help predict that class.

The analysis for the orientation of the incoming weights is far more complicated. We can start by noting:

Proposition 4.2. *For a fixed gating pattern \vec{g}_α , the fixed points for the outgoing weight vector $\theta_{\alpha,i}^*$ are given by $\theta_{\alpha,i}^* = \theta_{\langle \vec{\gamma}_\alpha^s \rangle, i} + n\pi$, with n a positive scalar.*

This can be derived directly from eq. 6. However, the vector $\langle \vec{\gamma}_\alpha^s \rangle$ depends on the values $\|\Delta \vec{y}^s\|$ (cfr. eq. 9), and due to the softmax function, these are nonlinear functions of the network parameters including $\theta_{\alpha,i}$ itself, as well as the parameters of the other neurons. In general, we can thus not find an explicit solution for $\theta_{\alpha,i}^*$. But we are here mainly interested in the directions of the incoming weight vectors in the period from initialization to right before the loss considerably drops, or equivalently, the period where

$\|\Delta \vec{y}^s\| \approx \frac{\sqrt{2}}{2}$ for all samples. It's insightful to compute a value for $\theta_{\alpha,i}^*$ in the case of a simplified system with fixed $\|\Delta \vec{y}^s\| = \frac{\sqrt{2}}{2}$ for all s (or at least all s in the effective dataset of the neuron). We find:

Proposition 4.3. *Assume $\vec{w}_\alpha^{(2)}$ is already aligned, i.e., $\phi_\alpha = \phi_\alpha^{*1}$ or $\phi_\alpha = \phi_\alpha^{*2}$. For a fixed gating pattern \vec{g}_α and when $\|\Delta \vec{y}^s\| = \frac{\sqrt{2}}{2}$ for all s in the effective dataset of the neuron, the target angle $\theta_{\alpha,i}^{*,\text{init}}$ is the angle of the vector:*

$$\vec{m}^1 \equiv N_1^e \langle \vec{x}^s \rangle_{C_1} - N_2^e \langle \vec{x}^s \rangle_{C_2} \text{ when } \phi_\alpha = \phi_\alpha^{*1} \quad (13)$$

$$\vec{m}^2 \equiv N_2^e \langle \vec{x}^s \rangle_{C_2} - N_1^e \langle \vec{x}^s \rangle_{C_1} \text{ when } \phi_\alpha = \phi_\alpha^{*2}. \quad (14)$$

In practice, of course, $\|\Delta \vec{y}^s\|$ does not remain at $\frac{\sqrt{2}}{2}$ and the loss eventually drops. $\|\Delta \vec{y}^s\| = \frac{\sqrt{2}}{2}$ corresponds to a zeroth order approximation to the nonlinear softmax function, and we can study what happens for higher order approximations (i.e., when $\|\Delta \vec{y}^s\|$ differs more and more from $\frac{\sqrt{2}}{2}$). In appendix E, we make use of the derivations made for a single neuron in (Refinetti et al., 2023), and show:

Proposition 4.4. *Assume the gating patterns are fixed, all outgoing weights have aligned, and the total set of effective datasets is disjoint. Under these assumptions, we can compute a series of corrections to $\theta_{\alpha,i}^*$ based on a Taylor expansion of the softmax function around 0. Importantly, as we start from small random initial conditions, each subsequent correction only becomes important later in training time. We furthermore find that the importance of higher order corrections depends on the presence of higher order moments of the distributions of the effective samples per class.*

This has two important consequences: first, early in training, we can make use of a zeroth order and possible first order approximation to the softmax function. In this stage, only the means and the variances of the effective datasets influence the target directions (we computed the first order correction in appendix E). As training progresses and the loss considerably drops, the target directions change based on the higher order statistics of the effective dataset (in line with results in (Atanasov et al., 2022)). For more complex datasets, the target directions will thus still change after the initial drop in the loss. For simple datasets like the one used for fig 2, the initial alignment remains the same.

This observation allows us furthermore to conjecture why, after some short initial phase in training, we can assume there exist groups of neurons with a shared and fixed gating vector (until the loss considerably drops for the samples in the corresponding effective dataset). Consider a group of neurons that have a similar orientation for their vectors $\vec{w}_\alpha^{(1)}$ at initialization. Their gating vectors might differ, but the difference is relatively small: as each bias is initialized as $b_\alpha = 0$, the gating vector is solely determined by the orientation of $\vec{w}_\alpha^{(1)}$ with respect to the samples \vec{x}^s . In the very beginning of learning, the target directions are given by the vectors \vec{m} (eq. 14), based on the means of the current effective dataset. The target directions will thus be similar, and therefore the different $\vec{w}_\alpha^{(1)}$ will converge to similar directions. As they rotate, their gating vectors become more and more similar, until the gating vector and effective dataset becomes shared and they follow the same dynamics given by the eqs. 4 - 8, and thus obtain the same target direction in the period before the loss drops.

4.3. Unlocking

Here we discuss how the cosine similarity between the weight vectors of neurons and their (initial) target directions ‘unlocks’ the growth in norm. We first note:

Proposition 4.5. *The ratio of gradient updates on angles vs. norms is proportional to:*

$$\frac{\frac{\partial L^s}{\partial (\phi_\alpha)}}{\frac{\partial L^s}{\partial \|\vec{w}_\alpha^{(2)}\|}} \sim \tan(\phi_{\Delta \vec{y}^s} - \phi_\alpha) \quad (15)$$

This means that when $\vec{w}_\alpha^{(2)}$ is far from its (current) target direction ($\phi_\alpha^* - \phi_\alpha \approx \frac{\pi}{2}$), it changes very fast in angle and very slowly norm (see fig. 3). A similar observation holds for $\theta_{\alpha,i}$.

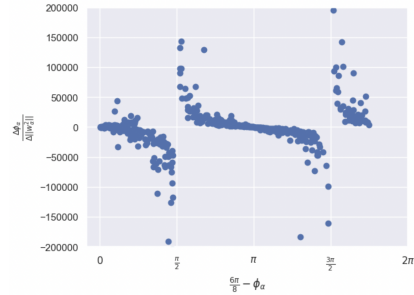


Figure 3. Ratio $\frac{\partial L^s}{\partial (\phi_\alpha)} / \frac{\partial L^s}{\partial \|\vec{w}_\alpha^{(2)}\|}$ in function of $\frac{3\pi}{4} - \phi_\alpha$ for the XOR-like experiment with 1000 hidden neurons at $t=0$. Note the values on the y-axis.

As we discussed before, this initial decoupling of norm updates from angle updates has been called ‘silent alignment’ (Atanasov et al., 2022), as vectors generally align to their initial target direction *before* their norms start to increase and the loss starts to drop. But, crucially and unlike assumed before, this decoupling is not a complete decoupling: while vectors that are ‘far’ away from their target direction will have a negligible increase in norm, vectors closer in direction to their target direction will already have a significant increase in norm. In fact, it’s more accurate to consider two phases: an initial phase, in which groups of weight vectors are very quickly converging to the neighborhood of a shared initial target direction; and an ‘unlocking’ phase, in which

vectors are close enough to their initial target direction to unlock a significant growth in norm, but they are not necessarily fully aligned.

We here continue with analyzing what happens in the unlocking phase for individual neurons, $\theta_{\alpha,i}$ is close but not equal to its target value. Let $\delta_{\alpha,i}$ be the remaining angular distance, $\delta_{\alpha,i} = \delta_{\alpha,i}(t) = |\theta_{\langle \vec{\gamma}_\alpha^s \rangle, i} - \theta_{\alpha,i}|$. We then obtain (details, see appendix F):

$$\frac{\partial L}{\partial \|\vec{w}_\alpha^{(1)}\|} = -\|\vec{w}_\alpha^{(2)}\| \|\langle \vec{\gamma}_\alpha^s \rangle\| \cos(\delta_\alpha) \quad (16)$$

$$\frac{\partial L}{\partial \|\vec{w}_\alpha^{(2)}\|} = -\|\vec{w}_\alpha^{(1)}\| \|\langle \vec{\gamma}_\alpha^s \rangle\| \cos(\delta_\alpha) \quad (17)$$

which is a coupled set of equations. But if we assume small initial conditions, slow learning rate (such that we can consider gradient flow), $\|\Delta \vec{y}^s\| \approx \frac{\sqrt{2}}{2}$ for all s in the effective dataset, $\vec{w}_\alpha^{(2)}$ aligned and $\delta_{\alpha,i}(t)$ changing slowly compared to the norms, we can find a simple differential equation for the product of norms $a_\alpha = \|\vec{w}_\alpha^{(2)}\| \|\vec{w}_\alpha^{(1)}\|$ (see appendix F):

$$\frac{\partial a_\alpha}{\partial t} = \lambda \|\langle \vec{\gamma}_\alpha^s \rangle\| \cos(\delta_\alpha) a_\alpha, \quad (18)$$

which leads to:

Proposition 4.6. Consider the product $a_\alpha = \|\vec{w}_\alpha^{(2)}\| \|\vec{w}_\alpha^{(1)}\|$. Under the assumptions as described above, we have for the product of norms $a_\alpha = \|\vec{w}_\alpha^{(2)}\| \|\vec{w}_\alpha^{(1)}\|$:

$$a_\alpha(t) \sim e^{\lambda \|\langle \vec{\gamma}_\alpha^s \rangle\| \cos(\delta_\alpha) t} \quad (19)$$

with $\|\langle \vec{\gamma}_\alpha^s \rangle\|$ and $\delta_{\alpha,i}(t)$ considered constants. This indicates that, right before the loss drops, neurons that are closer to their target direction grow exponentially faster in norm. Here ‘closeness’ is measured by cosine similarity between $\vec{w}_\alpha^{(1)}$ and $\langle \vec{\gamma}_\alpha^s \rangle$.

In fact, we have so far shown that the norms considerably increase closer to the target direction; in appendix G, we show that this increase indeed leads to a drop in the loss.

4.4. Racing

Let's now discuss how the growth of the norm for one neuron relates to the growth of the norms for other neurons. Consider a group of neurons where each incoming weight vector is approximately, but not fully, aligned to a shared target direction (i.e., a group of neurons in the unlocking phase). We assume their outgoing weight vectors are fully aligned. We have an equation for $\frac{\partial a_\beta}{\partial t}$ for each neuron of the group indexed by β , but the vector $\langle \vec{\gamma}_\beta^s \rangle$ is shared. We therefore drop the subscript β , thus $\langle \vec{\gamma}_\beta^s \rangle = \langle \vec{\gamma}^s \rangle$, for this section. We thus have a set of equations

$$\frac{\partial a_\beta}{\partial t} = \lambda \|\langle \vec{\gamma}^s \rangle(t)\| \cos(\delta_\beta) a_\beta, \quad (20)$$

with

$$\langle \vec{\gamma}^s \rangle(t) = \frac{N_1^e}{N^e} \langle \|\Delta \vec{y}^s\|(t) \vec{x}^s \rangle_{C_1} - \frac{N_2^e}{N^e} \langle \|\Delta \vec{y}^s\|(t) \vec{x}^s \rangle_{C_2} \quad (21)$$

where we have assumed $\phi_\beta = \phi_\beta^{1*} = \frac{7\pi}{4}$ for all β , but the other case is similar. $\langle \vec{\gamma}^s \rangle(t)$ depends on training time through the evolution of the error vectors $\Delta \vec{y}^s(t)$. As discussed above, initially, we can assume all $\|\Delta \vec{y}^s\| \approx \frac{\sqrt{2}}{2}$, which leads to an exponential difference between the growth of the norms of the neurons, see eq. 19.

However, as training progresses, the norm of the error vectors $\|\Delta \vec{y}^s\|$ decreases. This means the growth in norms slows down (eq. 20 and 21), and is no longer exponential. There is a crucial thing to note here: the neurons that are closest to the target directions obtain the highest norms, therefore contribute most to the decrease in error vectors and loss, and the decreased loss subsequently slows down the learning for *all* neurons of the group (eq. 20). This can be seen as a kind of race between neurons: the neurons that arrive first near the target direction exponentially grow in norm compared to those further away, and those early arriving neurons are the ones mainly solving the effective task (i.e., the task defined by the effective dataset) through reducing the loss. In other words, they win the race to become the important neurons in solving this specific (sub)task.

4.5. Effective Capacity and Redundancy

We can now explain the first way in which gradient descent reduces the effective capacity: when (exactly) mutually aligned, neurons can be merged without affecting the computations of the network. Consider two neurons indexed by α and β that have the same direction of their total parameter vector. Then we can compute an effective norm: $\|\mathbf{w}_{\text{effective}}^{\text{tot}}\| = \sqrt{\|\mathbf{w}_\alpha^{\text{tot}}\|^2 + \|\mathbf{w}_\beta^{\text{tot}}\|^2}$ to merge the two neurons without affecting the predictions and loss. In general, alignment should be seen as the projection of weight vectors to a lower, task-dependent subspace, see e.g., (Gur-Ari et al., 2018; Saxe et al., 2019). In our binary classification setting, the subspaces are one-dimensional, such that weight vectors align to the actual target directions (which corresponds to monosemanticity) and we can straightforwardly compute the resulting equivalent neuron from their respective norms.

4.6. Effective Capacity and Lottery Tickets

Beneficial initial conditions In our framework, a neuron becomes a ‘winning ticket’ in a group of neurons if it is closer aligned to the shared target direction in the unlocking phase, i.e., $\delta_{\alpha,i}(t_u) = |\theta_{\langle \vec{\gamma}_\alpha^s \rangle, i}(t_u) - \theta_{\alpha,i}(t_u)|$ is small for all i compared to the other neurons of the group (see eq. 20). Here we use t_u to indicate the start of the unlocking phase. This thus allows us to characterize the beneficial

initial conditions of lottery tickets: consider a group of neurons, that, in the unlocking phase, will have a shared target direction for their $\vec{w}_\alpha^{(1)}$. We assume their outgoing weights will be fully aligned before the start of this unlocking phase. The beneficial initial conditions that would make a neuron a ‘winning ticket’ are then these initializations that lead to a smaller $\delta_{\alpha,i}(t_u)$ compared to the other neurons in the group. In principle, there is no way to exactly predict this at initialization, as we would need to know the evolution of the neurons and their gating vectors in the first steps of training to exactly predict each $\delta_{\alpha,i}(t_u)$. However, we find experimentally that the angular distance at $t=t_0$, thus $\delta_{\alpha,i}(t_0) = |\theta_{\langle \vec{\gamma}_\alpha^s \rangle, i}(t_0) - \theta_{\alpha,i}(t_0)|$, is already predictive of the final relative norm of each neuron (see fig. 1 and experimental section).

The Selection Mechanism The core of the Lottery Ticket Conjecture is the massive disparity between the final norms of ‘winning’ vs. ‘losing’ weights. We explain this via the exponential solution to the norm dynamics (eq. 19). Consider two neurons, α (well-aligned) and β (poorly aligned), i.e., $\cos(\delta_\alpha) > \cos(\delta_\beta)$ at the start of the unlocking phase. During this early phase where the loss is high ($\|\Delta \vec{y}^s\| \approx \text{const}$), the ratio of their norms evolves as $\frac{a_\alpha(t)}{a_\beta(t)} \sim e^{\lambda \|\gamma\| (\cos \delta_\alpha - \cos \delta_\beta) t}$. This indicates that even a marginal advantage in initial alignment is amplified exponentially. This explains why researchers find that ‘winning tickets’ can be identified very early in training (Frankle et al., 2020b): the race is often decided in the first few iterations, before the loss drops significantly. The Racing principle furthermore explains why the ‘losing tickets’ do not eventually catch up. As the ‘winning’ neurons align and grow in norm, they begin to solve the task, causing the error to decrease (see Section 4.7). The ‘winners’ effectively starve the ‘losers’ of the gradient updates needed to either align or grow. This leads to the observed sparsity in overparameterized networks: a small subset of neurons (the winning tickets) accounts for the majority of the total weight norm, while the rest remain closer near their initialization values. However, the more complex the dataset, the more task-relevant directions are needed to solve the task; this means the same amount of neurons is divided over a larger set of races, and fewer neurons take part in each separate race. This leads to less pronounced differences in magnitude and less sparsity.

Why we cannot fully predict lottery tickets early in training We can identify at least two reasons why it is not possible to fully predict lottery tickets at single timepoints early in training. The first one is related to the asynchronous learning speeds of different neuron groups. While the ‘race’ occurs within aligned groups, learning rates can vary significantly *between* groups because the effective learning rate is determined by $\|\langle \vec{\gamma}_\alpha^s \rangle\|$ (eq. 9), which is in itself determined by both the norms and the number of samples in the effec-

tive dataset of the neuron. As demonstrated in fig. 2, groups processing samples with lower norms align and reduce loss much later than others. Consequently, a neural network is best viewed as a collection of overlapping subsystems evolving at different scales. In practice, norm-based pruning at a fixed time early in training may therefore prematurely discard “slow” groups that have yet to enter their unlocking phase, removing the capacity required for specific sub-tasks. Furthermore, once the loss starts to drop, the dynamics can considerably change: as the biases grow (see eq. 8), the gating vectors change; and for complex effective datasets with higher order statistical moments, the target directions also change. We can, e.g., envision the case where neurons that were previously unfavorably aligned, now become favorably aligned to new the updated target directions. While the gradients and thus speed of learning are generally smaller during this period, such neurons could potentially still ‘catch up’ with neurons that obtained a higher norm early in training and become part of the lottery ticket later in training.

5. Experiments

Initialization scale Before discussing experiments with CIFAR10 data, we illustrate the role of the initialization scale on alignment with a simple experiment using a XOR dataset and 500 neurons. In fig. 4, we plot the directions of the incoming weight vectors over training (the colors correspond to their target direction) for different initialization scales (std of the gaussian). Increasing the initialization scale clearly reduces the tendency to align, which is in line with the fact that increasing initialization scale moves the dynamics from the rich, feature learning regime to the lazy regime (Woodworth et al., 2020).

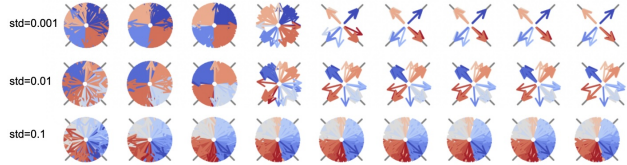


Figure 4. Illustration of the alignment of incoming weight vectors during training for different initialization scales.

Settings We create binary classification datasets from CIFAR-10 images: the first class has an equal number of samples of the original classes ‘airplane’ and ‘cat’, the second class has an equal number of samples of ‘car’ and ‘bird’. We use grayscale images and flatten the images to obtain 1024×1 input vectors. We then consider a network with 250 neurons and three experimental settings: (1) 200 samples, batch size 4, (overparameterized/low scale init); (2) 200 samples, batch size 4, $std = 0.01$ (overparameterized/normal scale init); and (3) 2000 samples, batch size 32, $std = 0.01$ (underparameterized/normal scale init).

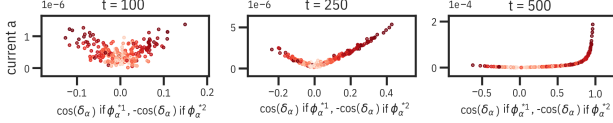


Figure 5. Illustration of the two larger subsystems of neurons evolving at different speeds. For the neurons which align to ϕ_α^{1*} we used the negative of their $\cos(\delta_\alpha)$ values, to be able to compare the groups as the left and right hand side within the same plot.

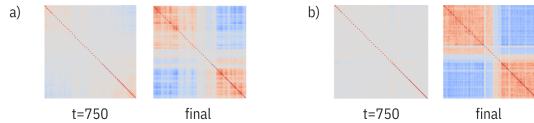


Figure 6. Cosine similarity matrices between the total parameter vectors of individual neurons at different timesteps during training, for experimental setting 2 (plot a) and 3 (plot b).

Here std is the standard deviation of the gaussian used to initialize all weights. The learning rate was set to $\lambda = 0.001$, and each network was trained with an SGD optimizer with momentum 0.9.

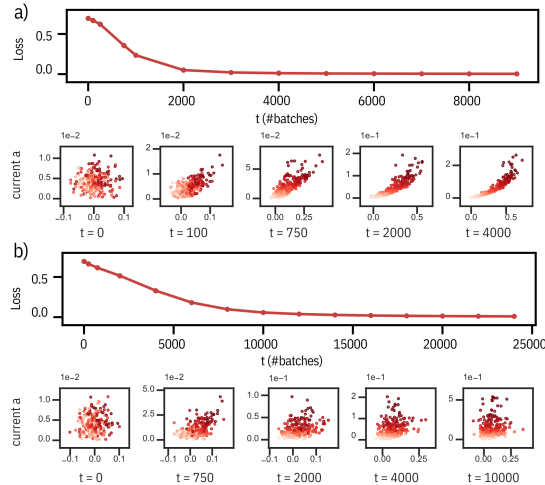


Figure 7. Loss and current alignment of incoming weights vs. current norm a_α over training time for experimental setting 2 (a) and experimental setting 3 (b). Neurons are colored according to their final norm, with a darker color indicating a higher final norm.

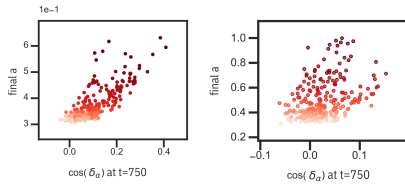


Figure 8. Current alignment of incoming weights vs. final norm a_α for experimental setting 2 (left) and experimental setting 3 (right). Neurons are colored according to their final norm.

Small initialization We have shown the results for the first experimental setting in fig. 1. In this setting, the initialization leads to a strong initial decoupling between the growth in norm and the growth in direction and thus a relatively

long plateau before the loss drops (see fig. 1a). Moreover, we can see a strong tendency to align to shared directions over time (fig. 1b). At the end of training, we can merge all neurons with a cosine similarity ≥ 0.999 and we obtain a network with 150 effective neurons, with an increase in the loss of merely 0.1%. Fig. 1c shows a very clear exponential growth of the norms a in function of $\cos(\delta_\alpha)$ right before the loss drops ($t=500$, lower left plot), which is what we predict from theory. However, we would like to return to the point of different groups of neurons evolving at different speeds. We can discern two ‘supergroups’ of neurons, depending on whether their outgoing weight vectors align to ϕ_α^{1*} or ϕ_α^{2*} . In fig. 5 we show neurons that align to ϕ_α^{1*} as before, but for neurons that align to ϕ_α^{2*} we use negative of their values for $\cos(\delta_\alpha)$, such that we can straightforwardly compare the evolution of the left hand side of the graph to the right hand side. We can clearly see that the group associated to ϕ_α^{2*} is evolving at a slightly slower pace; the total system shown in fig. 1 is thus a combination of at least two subsystems evolving at slightly different speeds. Nevertheless, even if we pick a single point in time ($t=500$) early in training, we can see in fig. 1 (lower row) that the values of δ_α at this timepoint predict very well which neurons will have the highest final norm values a_α . **Normal initialization** We subsequently reduce the initialization scale to the more conventional value of $std = 0.01$. Results are shown in fig. 6a and fig. 7a. The tendency to align reduces, and neurons can no longer be merged without affecting the loss. The initial plateau in the loss disappears, and the exponential growth behavior is less clearly defined, but it is still present. The values of $\cos(\delta_\alpha)$ early in training still correlate to a large degree to the final values of a , as can be seen in fig. 8 (left). **Larger dataset** We then also increase the complexity of the dataset through increasing the dataset size. In this case, the network becomes underparameterized (in the conventional sense of less parameters than samples) and we expect that gradient descent would reduce the effective capacity to a lesser degree. While the alignment is stronger compared to setting 2 (fig. 6), we also cannot merge neurons without affecting the loss. We find that the exponential growth behavior is even less defined, indicating this network will show less of a difference between ‘winning tickets’ and ‘losing tickets’, i.e., it will be harder to prune. But the angular distances are still predictive of final norm (fig. 7 b) and fig. 8 right).

6. Conclusion

In this paper, we have analyzed the dynamics of gradient descent at the level of individual neurons in single hidden layer ReLU networks for binary classification. We identified three dynamical principles, mutual alignment, unlocking and racing, that allowed us to explain how gradient descent adapts a network’s theoretical capacity to the task. We specifically

showed (in line with earlier work) why some neurons mutually align to a shared, task-related target direction, after which they can be merged to a single equivalent neuron. Our main contributions, however, are the insights in the lottery ticket conjecture. We explained that the beneficial initial conditions of lottery tickets are in fact their favorable initial alignment to task-related target directions. And we identified the lottery selection mechanism as a race between neurons early in training that arises because neurons that align faster to their target direction obtain an exponentially higher norm. Our results can serve as a theoretical basis to explain a range of earlier observations about lottery tickets: they can be largely predicted early in training (Frankle et al., 2020b;a); the sign of the initialization (hence, the orientation) is more important than the values (Zhou et al., 2019); and as we found the tickets consist of neurons closely aligned to task-relevant directions, they can generalize across similar datasets (Morcos et al., 2019). With more extensions of our framework to advanced architectures, it could serve as a basis to understand capacity and sparsity in large, modern neural networks.

7. Impact statement

This paper presents work whose goal is to advance the field of machine learning. There are many potential societal consequences of our work, none of which we feel must be specifically highlighted here.

References

Advani, M. S., Saxe, A. M., and Sompolsky, H. High-dimensional dynamics of generalization error in neural networks. *Neural Networks*, 132:428–446, December 2020. ISSN 08936080. doi: 10.1016/j.neunet.2020.08.022. URL <https://linkinghub.elsevier.com/retrieve/pii/S0893608020303117>.

Atanasov, A., Bordelon, B., and Pehlevan, C. Neural Networks as Kernel Learners: The Silent Alignment Effect. *The Tenth International Conference on Learning Representations, ICLR*, 2022.

Baratin, A., George, T., Laurent, C., Hjelm, R. D., Lajoie, G., Vincent, P., and Lacoste-Julien, S. Implicit regularization via neural feature alignment. In Banerjee, A. and Fukumizu, K. (eds.), *The 24th International Conference on Artificial Intelligence and Statistics, AISTATS 2021, April 13-15, 2021, Virtual Event*, volume 130 of *Proceedings of Machine Learning Research*, pp. 2269–2277. PMLR, 2021. URL <http://proceedings.mlr.press/v130/baratin21a.html>.

Behnke, M. and Heafield, K. Losing Heads in the Lottery: Pruning Transformer Attention in Neural Machine Translation. In *Proceedings of the 2020 Conference on Empirical Methods in Natural Language Processing (EMNLP)*, pp. 2664–2674, Online, 2020. Association for Computational Linguistics. doi: 10.18653/v1/2020.emnlp-main.211. URL <https://www.aclweb.org/anthology/2020.emnlp-main.211>.

Brix, C., Bahar, P., and Ney, H. Successfully Applying the Stabilized Lottery Ticket Hypothesis to the Transformer Architecture, July 2020. URL <http://arxiv.org/abs/2005.03454>. arXiv:2005.03454 [cs].

Cheng, H., Zhang, M., and Shi, J. Q. A survey on deep neural network pruning: Taxonomy, comparison, analysis, and recommendations. *IEEE Transactions on Pattern Analysis and Machine Intelligence*, 46(12):10558–10578, 2024. doi: 10.1109/TPAMI.2024.3447085.

Du, S. S. and Lee, J. D. On the Power of Overparametrization in Neural Networks with Quadratic Activation. *Proceedings of the 35th International Conference on Machine Learning*, 2018.

Frankle, J. and Carbin, M. The Lottery Ticket Hypothesis: Finding Sparse, Trainable Neural Networks, March 2019. URL <http://arxiv.org/abs/1803.03635>. arXiv:1803.03635 [cs].

Frankle, J., Dziugaite, G. K., Roy, D. M., and Carbin, M. Linear Mode Connectivity and the Lottery Ticket Hypothesis. 2020a.

Frankle, J., Schwab, D. J., and Morcos, A. S. The Early Phase of Neural Network Training, February 2020b. URL <http://arxiv.org/abs/2002.10365>. arXiv:2002.10365 [cs].

Frantar, E. and Alistarh, D. Sparsegpt: Massive language models can be accurately pruned in one-shot. In Krause, A., Brunskill, E., Cho, K., Engelhardt, B., Sabato, S., and Scarlett, J. (eds.), *International Conference on Machine Learning, ICML 2023, 23-29 July 2023, Honolulu, Hawaii, USA*, volume 202 of *Proceedings of Machine Learning Research*, pp. 10323–10337. PMLR, 2023. URL <https://proceedings.mlr.press/v202/frantar23a.html>.

Fukai, T. and Tanaka, S. A simple neural network exhibiting selective activation of neuronal ensembles: from winner-take-all to winners-share-all. *Neural computation*, 9(1):77–97, 1997.

Gidel, G., Bach, F., and Lacoste-Julien, S. Implicit Regularization of Discrete Gradient Dynamics in Linear Neural Networks. *33rd Conference on Neural Information Processing Systems (NeurIPS 2019)*, 2019.

Gur-Ari, G., Roberts, D. A., and Dyer, E. Gradient Descent Happens in a Tiny Subspace, December 2018. URL <http://arxiv.org/abs/1812.04754>. arXiv:1812.04754 [cs].

Hoefer, T., Alistarh, D., Ben-Nun, T., and Dryden, N. Sparsity in Deep Learning: Pruning and growth for efficient inference and training in neural networks. *Journal of Machine Learning Research*, 23:1–124, 2021.

J Dominé, C. C., Braun, L., Fitzgerald, J. E., and Saxe, A. M. Exact learning dynamics of deep linear networks with prior knowledge *. *Journal of Statistical Mechanics: Theory and Experiment*, 2023(11):114004, November 2023. ISSN 1742-5468. doi: 10.1088/1742-5468/ad01b8. URL <https://iopscience.iop.org/article/10.1088/1742-5468/ad01b8>.

Jarvis, D., Klein, R., Rosman, B., and Saxe, A. M. Make Haste Slowly: A Theory of Emergent Structured Mixed Selectivity in Feature Learning ReLU Networks. *The Thirteenth International Conference on Learning Representations, {ICLR}*, 2025.

Ji, Z. and Telgarsky, M. Directional convergence and alignment in deep learning. *Advances in Neural Information Processing Systems*, 33:17176–17186, 2020.

Kopitkov, D. and Indelman, V. Neural Spectrum Alignment: Empirical Study, April 2020. URL <http://arxiv.org/abs/1910.08720>. arXiv:1910.08720 [cs].

Lee, N., Ajanthan, T., and Torr, P. H. S. SNIP: Single-shot Network Pruning based on Connection Sensitivity, February 2019. URL <http://arxiv.org/abs/1810.02340>. arXiv:1810.02340 [cs].

Liu, B., Zhang, Z., He, P., Wang, Z., Xiao, Y., Ye, R., Zhou, Y., Ku, W.-S., and Hui, B. A Survey of Lottery Ticket Hypothesis, March 2024. URL <http://arxiv.org/abs/2403.04861>. arXiv:2403.04861 [cs].

Malach, E., Yehudai, G., Shalev-Schwartz, S., and Shamir, O. Proving the lottery ticket hypothesis: Pruning is all you need. In *International Conference on Machine Learning*, pp. 6682–6691. PMLR, 2020.

Morcos, A., Yu, H., Paganini, M., and Tian, Y. One ticket to win them all: generalizing lottery ticket initializations across datasets and optimizers. *Advances in neural information processing systems* 32, 2019.

Nacson, M. S., Lee, J. D., Gunasekar, S., Savarese, P. H. P., Srebro, N., and Soudry, D. Convergence of Gradient Descent on Separable Data. *Proceedings of the 22nd International Conference on Artificial Intelligence and Statistics (AISTATS)*, 2019.

Neyshabur, B., Tomioka, R., and Srebro, N. In Search of the Real Inductive Bias: On the Role of Implicit Regularization in Deep Learning, April 2015. URL <http://arxiv.org/abs/1412.6614>. arXiv:1412.6614 [cs, stat].

Paccat, J., Petrini, L., Geiger, M., Tyloo, K., and Wyart, M. Geometric compression of invariant manifolds in neural nets. *Journal of Statistical Mechanics: Theory and Experiment*, 2021(4):044001, April 2021. ISSN 1742-5468. doi: 10.1088/1742-5468/abf1f3. URL <http://arxiv.org/abs/2007.11471>. arXiv:2007.11471 [cs].

Paul, M., Chen, F., Larsen, B. W., Frankle, J., Ganguli, S., and Dziugaite, G. K. Unmasking the lottery ticket hypothesis: What's encoded in a winning ticket's mask? *arXiv preprint arXiv:2210.03044*, 2022.

Pellegrini, F. and Biroli, G. Neural network pruning denoises the features and makes local connectivity emerge in visual tasks. In *International conference on machine learning*, pp. 17601–17626. PMLR, 2022.

Pinson, H., Lenaerts, J., and Ginis, V. Linear CNNs Discover the Statistical Structure of the Dataset Using Only the Most Dominant Frequencies. In *International Conference on Machine Learning, ICML 2023, 23–29 July 2023, Honolulu, Hawaii, USA*, volume 202 of *Proceedings of Machine Learning Research*, pp. 27876–27906. PMLR, 2023. URL <https://proceedings.mlr.press/v202/pinson23a.html>.

Redman, W. T., Wang, Z., Ingrosso, A., and Goldt, S. On How Iterative Magnitude Pruning Discovers Local Receptive Fields in Fully Connected Neural Networks, March 2025. URL <http://arxiv.org/abs/2412.06545>. arXiv:2412.06545 [cs].

Refinetti, M., Ingrosso, A., and Goldt, S. Neural networks trained with SGD learn distributions of increasing complexity. In *International Conference on Machine Learning, PMLR*, 2023.

Saxe, A. M., McClelland, J. L., and Ganguli, S. A mathematical theory of semantic development in deep neural networks. *Proceedings of the National Academy of Sciences*, 116(23):11537–11546, June 2019. ISSN 0027-8424, 1091–6490. doi: 10.1073/pnas.1820226116. URL <https://pnas.org/doi/full/10.1073/pnas.1820226116>.

Saxe, A. M., Sodhani, S., and Lewallen, S. The Neural Race Reduction: Dynamics of Abstraction in Gated Networks. In *International Conference on Machine Learning, PMLR*, 2022.

Soudry, D., Hoffer, E., Nacson, M. S., Gunasekar, S., and Srebro, N. The Implicit Bias of Gradient Descent on Separable Data. *J. Mach. Learn. Res.*, 19:70:1–70:57, 2018.

Tachet, R., Pezeshki, M., Shabanian, S., Courville, A., and Bengio, Y. On the Learning Dynamics of Deep Neural Networks, December 2020. URL <http://arxiv.org/abs/1809.06848>. arXiv:1809.06848 [cs, stat].

Tarmoun, S., França, G., Haeffele, B., and Vidal, R. Understanding the Dynamics of Gradient Flow in Overparameterized Linear Models. *International Conference on Machine Learning, PMLR 139*, 2021.

Wang, C., Zhang, G., and Grosse, R. Picking Winning Tickets Before Training by Preserving Gradient Flow, August 2020. URL <http://arxiv.org/abs/2002.07376>. arXiv:2002.07376 [cs].

Woodworth, B., Gunasekar, S., Lee, J. D., Moroshko, E., Savarese, P., Golan, I., Soudry, D., and Srebro, N. Kernel and Rich Regimes in Overparametrized Models, July 2020. URL <http://arxiv.org/abs/2002.09277>. arXiv:2002.09277 [cs, stat].

Zhou, H., Lan, J., Liu, R., and Yosinski, J. Deconstructing lottery tickets: Zeros, signs, and the supermask. *Advances in neural information processing systems*, 32, 2019.

Zhu, M. and Gupta, S. To prune, or not to prune: exploring the efficacy of pruning for model compression, November 2017. URL <http://arxiv.org/abs/1710.01878>. arXiv:1710.01878 [stat].

A. Illustration of toy dataset

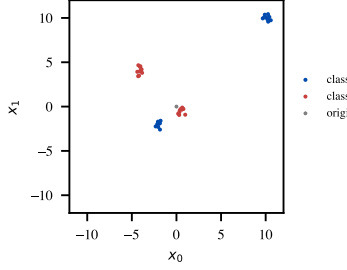


Figure 9. Toy dataset consisting of 4 Gaussian clusters, 2 for each class, where each cluster has a different magnitude of its centroid. The dataset is not linearly separable.

B. Equations of gradient descent

We want to analyze the gradient of the loss with respect to the angles and norms of the ingoing and outgoing weight vectors of each neuron. To achieve this, we start with computing the components of the gradient of the loss L^s with respect to the logits z_k^s , for an input sample s . These are given by the simple expression:

$$\frac{\partial L^s}{\partial z_k} = -(y_k^s - \hat{y}_k^s) = -\Delta y_k^s \quad (22)$$

due to the interaction between the cross-entropy loss and the softmax function. This gradient is then propagated to the outgoing weights of each neuron. We obtain:

$$\left(\frac{\partial L^s}{\partial \vec{w}_\alpha^{(2)}} \right)^T = -g_\alpha^s \Delta \vec{y}^s h_\alpha^s \quad (23)$$

and

$$\frac{\partial L^s}{\partial h_\alpha^s} = -g_\alpha^s \|\Delta \vec{y}^s\| \|\vec{w}_\alpha^{(2)}\| \cos(\phi_{\Delta y^s} - \phi_\alpha) \quad (24)$$

Using the chain rule:

$$\frac{\partial L}{\partial \|v\|} = \frac{\partial L}{\partial v_x} \frac{\partial v_x}{\partial \|v\|} + \frac{\partial L}{\partial v_y} \frac{\partial v_y}{\partial \|v\|} \quad (25)$$

$$\frac{\partial L}{\partial \theta} = \frac{\partial L}{\partial v_x} \frac{\partial v_x}{\partial \theta} + \frac{\partial L}{\partial v_y} \frac{\partial v_y}{\partial \theta} \quad (26)$$

together with the identities $\sin(a - b) = \sin(a)\cos(b) - \cos(a)\sin(b)$ and $\cos(a - b) = \cos(a)\cos(b) + \sin(a)\sin(b)$, and after averaging over the effective dataset, we arrive at:

$$\langle \frac{\partial L^s}{\partial \phi_\alpha} \rangle = -\langle h_\alpha^s \|\Delta \vec{y}^s\| \|\vec{w}_\alpha^{(2)}\| \sin(\phi_{\Delta y^s} - \phi_\alpha) \rangle \quad (27)$$

$$\langle \frac{\partial L^s}{\partial \|\vec{w}_\alpha^{(2)}\|} \rangle = -\langle h_\alpha^s \|\Delta \vec{y}^s\| \cos(\phi_{\Delta y^s} - \phi_\alpha) \rangle \quad (28)$$

$$(29)$$

For the derivatives to $\|\vec{w}_\alpha^{(1)}\|$ and $\theta_{\alpha,i}$, we use:

$$\frac{\partial L^s}{\partial \|\vec{w}_\alpha^{(1)}\|} = \frac{\partial L^s}{\partial h_\alpha^s} \frac{\partial h_\alpha^s}{\partial \|\vec{w}_\alpha^{(1)}\|} = \frac{\partial L^s}{\partial h_\alpha^s} \frac{\partial (\vec{w}_\alpha^{(1)} \cdot \vec{x}^s)}{\partial \|\vec{w}_\alpha^{(1)}\|} \quad (30)$$

Using the linearity of the derivative, we can move the factors of $\frac{\partial L^s}{\partial h_\alpha^s}$ to the inner product, and obtain:

$$\langle \frac{\partial L^s}{\partial(\theta_{\alpha,i})} \rangle = -\|\vec{w}_\alpha^{(2)}\| \frac{\partial \vec{w}_\alpha^{(1)} \cdot \langle \vec{\gamma}_\alpha^s \rangle}{\partial(\theta_{\alpha,i})} \quad (31)$$

$$\langle \frac{\partial L^s}{\partial \|\vec{w}_\alpha^{(1)}\|} \rangle = -\|\vec{w}_\alpha^{(2)}\| \frac{\partial \vec{w}_\alpha^{(1)} \cdot \langle \vec{\gamma}_\alpha^s \rangle}{\partial \|\vec{w}_\alpha^{(1)}\|} \quad (32)$$

with

$$\langle \vec{\gamma}_\alpha^s \rangle = \frac{1}{N} \sum_s^N g_\alpha^s \cos(\phi_{\Delta y^s} - \phi_\alpha) \|\Delta \vec{y}^s\| \vec{x}^s. \quad (33)$$

The derivative with respect to the bias is given by:

$$\langle \frac{\partial L^s}{\partial b_\alpha} \rangle = \langle \frac{\partial L^s}{\partial h_\alpha^s} \frac{\partial h_\alpha^s}{\partial b_\alpha} \rangle = -\|\vec{w}_\alpha^{(2)}\| \langle \|\Delta \vec{y}^s\| \cos(\phi_{\Delta y^s} - \phi_\alpha) \rangle \quad (34)$$

In total, this yields:

$$\langle \frac{\partial L^s}{\partial \phi_\alpha} \rangle = -\|\vec{w}_\alpha^{(2)}\| \langle h_\alpha^s \|\Delta \vec{y}^s\| \sin(\phi_{\Delta y^s} - \phi_\alpha) \rangle \quad (35)$$

$$\langle \frac{\partial L^s}{\partial \|\vec{w}_\alpha^{(2)}\|} \rangle = -\langle h_\alpha^s \|\Delta \vec{y}^s\| \cos(\phi_{\Delta y^s} - \phi_\alpha) \rangle \quad (36)$$

$$\langle \frac{\partial L^s}{\partial(\theta_{\alpha,i})} \rangle = -\|\vec{w}_\alpha^{(2)}\| \|\vec{w}_\alpha^{(1)}\| \|\langle \vec{\gamma}_\alpha^s \rangle\| \sin(\theta_{\langle \vec{\gamma}_\alpha^s \rangle, i} - \theta_{\alpha,i}) \quad (37)$$

$$\langle \frac{\partial L^s}{\partial \|\vec{w}_\alpha^{(1)}\|} \rangle = -\|\vec{w}_\alpha^{(2)}\| \|\langle \vec{\gamma}_\alpha^s \rangle\| \cos(\theta_{\langle \vec{\gamma}_\alpha^s \rangle, i} - \theta_{\alpha,i}) \quad (38)$$

$$\langle \frac{\partial L^s}{\partial b_\alpha} \rangle = -\|\vec{w}_\alpha^{(2)}\| \langle \|\Delta \vec{y}^s\| \cos(\phi_{\Delta y^s} - \phi_\alpha) \rangle \quad (39)$$

C. Computation of fixed points

C.1. Direction of outgoing weights

C.1.1. THE DIRECTION OF THE GRADIENT VECTORS IS FIXED

As the predicted output \hat{y}^s is normalized through the softmax, we can write it as $\hat{y}^s = [p, 1-p]^T$, for some $p^s \in [0, 1]$ depending on the timestep t. We thus obtain

$$\Delta y^s = \begin{bmatrix} 1 \\ 0 \end{bmatrix} - \begin{bmatrix} p \\ 1-p \end{bmatrix} = \begin{bmatrix} 1-p \\ -(1-p) \end{bmatrix} \text{ or } \Delta y^s = \begin{bmatrix} 0 \\ 1 \end{bmatrix} - \begin{bmatrix} p \\ 1-p \end{bmatrix} = \begin{bmatrix} -p \\ p \end{bmatrix}, \quad (40)$$

This means that while the magnitude of the vectors Δy^s can change during training, their directions stay constant. The angles $\phi_{\Delta y^s}$ are thus fixed at $\phi_{\Delta y^s} = \frac{7\pi}{4}$ for samples of the first class, and at $\phi_{\Delta y^s} = \frac{3\pi}{4}$ for samples of the second class.

C.1.2. TARGET DIRECTIONS

We can then determine the final angles ϕ_α^* the angles ϕ_α will converge to from computing the so-called fixed points of Eq. (3). This means we determine the ϕ_α^* for which $\frac{\partial \phi_\alpha^*}{\partial t} = -\lambda \langle \frac{\partial L^s}{\partial \phi_\alpha^*} \rangle = 0$. We repeat the needed equation here for convenience:

$$-\lambda \langle \frac{\partial L^s}{\partial \phi_\alpha} \rangle = \lambda \|\vec{w}_\alpha^{(2)}\| \langle h_\alpha^s \|\Delta \vec{y}^s\| \sin(\phi_{\Delta y^s} - \phi_\alpha) \rangle \quad (41)$$

Let $s \in C_1$ be the indices for samples of the first class, and $s' \in C_2$ be the indices for the second class. If we write the sums

over the effective samples per class explicitly, we obtain that the following must hold:

$$\sum_{s \in C_1} g_\alpha^s h_\alpha^s \|\Delta y^s\| \sin\left(\frac{7\pi}{4} - \phi_\alpha^*\right) + \sum_{s' \in C_2} g_\alpha^{s'} h_\alpha^{s'} \|\Delta y^{s'}\| \sin\left(\frac{3\pi}{4} - \phi_\alpha^*\right) = 0 \quad (42)$$

$$\iff \left[- \sum_{s \in C_1} g_\alpha^s h_\alpha^s \|\Delta y^s\| + \sum_{s' \in C_2} g_\alpha^{s'} h_\alpha^{s'} \|\Delta y^{s'}\| \right] \sin\left(\frac{3\pi}{4} - \phi_\alpha^*\right) = 0. \quad (43)$$

The first factor is very unlikely to be exactly zero in practice, so we arrive at:

$$\phi_\alpha^* = \frac{3\pi}{4} + n\pi. \quad (44)$$

Which of these possible fixed points, given by the sets $\frac{3\pi}{4} + 2n\pi$ and $\frac{7\pi}{4} + 2n\pi$, will the angle converge to? To answer this question, we can determine their stability through the second derivative. We have to determine whether the expression:

$$- \left(\sum_{s \in C_1} g_\alpha^s h_\alpha^s \|\Delta y^s\| \cos\left(\frac{7\pi}{4} - \phi_\alpha^*\right) + \sum_{s' \in C_2} g_\alpha^{s'} h_\alpha^{s'} \|\Delta y^{s'}\| \cos\left(\frac{3\pi}{4} - \phi_\alpha^*\right) \right) \quad (45)$$

$$(46)$$

amounts to a positive (unstable fixed point) or negative value (stable fixed point). Let's start with the case $\phi_\alpha^* = \frac{7\pi}{3} + n\pi$. We find:

$$- \left(\sum_{s \in C_1} g_\alpha^s h_\alpha^s \|\Delta y^s\| - \sum_{s' \in C_2} g_\alpha^{s'} h_\alpha^{s'} \|\Delta y^{s'}\| \right) < 0 \quad (47)$$

$$\iff \left(\sum_{s \in C_1} g_\alpha^s h_\alpha^s \|\Delta y^s\| - \sum_{s' \in C_2} g_\alpha^{s'} h_\alpha^{s'} \|\Delta y^{s'}\| \right) > 0 \quad (48)$$

$$\iff \sum_{s \in C_1} g_\alpha^s h_\alpha^s \|\Delta y^s\| > \sum_{s' \in C_2} g_\alpha^{s'} h_\alpha^{s'} \|\Delta y^{s'}\| \quad (49)$$

In other words, when $\sum_{s \in C_1} g_\alpha^s h_\alpha^s \|\Delta y^s\| > \sum_{s' \in C_2} g_\alpha^{s'} h_\alpha^{s'} \|\Delta y^{s'}\|$, $\phi_\alpha^* = \frac{7\pi}{4} + n\pi$ is the stable fixed point. When the reverse holds, $\phi_\alpha^* = \frac{3\pi}{4} + n\pi$ is the stable fixed point.

C.2. Direction of incoming weights

$$\frac{\partial \theta_{\alpha,i}^*}{\partial t} = -\lambda \left\langle \frac{\partial L^s}{\partial \theta_{\alpha,i}^*} \right\rangle = 0 \quad (50)$$

$$\iff \lambda \|\bar{w}_\alpha^{(2)}\| \|\bar{w}_\alpha^{(1)}\| \|\langle \vec{\gamma}_\alpha^s \rangle\| \sin(\theta_{\langle \vec{\gamma}_\alpha^s \rangle, i} - \theta_{\alpha,i}) = 0 \quad (51)$$

$$\iff \sin(\theta_{\langle \vec{\gamma}_\alpha^s \rangle, i} - \theta_{\alpha,i}) = 0 \quad (52)$$

$$\iff \theta_{\alpha,i} = \theta_{\langle \vec{\gamma}_\alpha^s \rangle, i} + n\pi. \quad (53)$$

The sign of $\frac{\partial^2 \theta_{\alpha,i}^*}{\partial t^2}$ is determined by the sign of

$$\cos(\theta_{\langle \vec{\gamma}_\alpha^s \rangle, i} - \theta_{\alpha,i}) \frac{\partial(\theta_{\langle \vec{\gamma}_\alpha^s \rangle, i} - \theta_{\alpha,i})}{\partial \theta_{\alpha,i}} \quad (54)$$

In the regime where $\|\Delta y^s\| \approx 0.5$ for all samples, $\theta_{\langle \vec{\gamma}_\alpha^s \rangle, i}$ does not depend on $\theta_{\alpha,i}$, and we obtain:

$$\text{a negative sign when } \theta_{\alpha,i} = \theta_{\langle \vec{\gamma}_\alpha^s \rangle, i} + n\pi \text{ with } n \text{ even} \quad (55)$$

$$\text{a positive sign when } \theta_{\alpha,i} = \theta_{\langle \vec{\gamma}_\alpha^s \rangle, i} + n\pi \text{ with } n \text{ odd} \quad (56)$$

this means $\theta_{\alpha,i} = \theta_{\langle \vec{\gamma}_\alpha^s \rangle, i} + 2n\pi$ is the stable fixed point (at least during the initial regime).

D. Approximations to the softmax

In general, we have for the output nodes:

$$\hat{y}_0 = \frac{e^{z_0^s}}{e^{z_0^s} + e^{z_1^s}} \quad (57)$$

$$\hat{y}_1 = \frac{e^{z_1^s}}{e^{z_0^s} + e^{z_1^s}} \quad (58)$$

$$(59)$$

When $\vec{w}_\alpha^{(2)}$ is aligned, we have either $\vec{w}_\alpha^{(2)} = k_\alpha \begin{bmatrix} 1 \\ -1 \end{bmatrix}$ or $\vec{w}_\alpha^{(2)} = k_\alpha \begin{bmatrix} -1 \\ 1 \end{bmatrix}$ for a positive scalar k_α . If all outgoing weights are aligned, we obtain:

$$z_0^s = \sum_{\alpha // class1} k_\alpha h_\alpha - \sum_{\alpha' // class2} k_{\alpha'} h_{\alpha'} \quad (60)$$

$$z_1^s = - \sum_{\alpha // class1} k_\alpha h_\alpha + \sum_{\alpha' // class2} k_{\alpha'} h_{\alpha'} \quad (61)$$

$$(62)$$

where $\alpha // class1$ means a sum over the neurons for which $\phi_\alpha = \phi_\alpha^{*1}$. We thus have, when all outgoing weights are aligned, that $z_1^s = -z_0^s$. The output can thus be described by keeping track of the first output node, and we define $\hat{p}^s = \hat{y}_0^s$. Then we can rewrite \hat{p}^s as:

$$\hat{p}^s = \frac{e^{z_0^s}}{e^{z_0^s} + e^{z_1^s}} = \frac{1}{1 + e^{-2z_0^s}} = \text{sigmoid}(2z_0^s) \quad (63)$$

We can expand the sigmoid function around the origin:

$$\text{sigmoid}(x) = \frac{1}{2} + \frac{1}{4}x - \frac{1}{48}x^3 + \dots \quad (64)$$

Thus, a first order approximation to \hat{p}^s is given by

$$\hat{p}^s \approx \frac{1}{2} + \frac{1}{2}z_0^s \quad (65)$$

This approximation is appropriate in the early phase of learning when starting from small initial conditions, as in this case z_0^s is small.

E. Approximations to the target directions of $\vec{w}_\alpha^{(1)}$

We here do a similar derivation as the one outlined in (Refinetti et al., 2023) for a single perceptron, but now for neuron within a larger network, where we assumed the outgoing weights are aligned. We consider the averaged derivative with respect to the weight vector $\vec{w}_\alpha^{(1)}$

$$\langle \frac{\partial L^s}{\partial \vec{w}_\alpha^{(1)}} \rangle = -||\vec{w}_\alpha^{(2)}|| \vec{\gamma}_\alpha \quad (66)$$

with γ_α :

$$\vec{\gamma}_\alpha = \sum_s g_\alpha^s \cos(\phi_{\Delta y^s} - \phi_\alpha) ||\Delta \vec{y}^s|| \vec{x}^s \quad (67)$$

The steady state for this equation is given by (see similar derivation in (Refinetti et al., 2023))

$$\vec{\gamma}_\alpha = 0 \quad (68)$$

and we can use then use the first order approximation eq. 65:

$$\|\Delta \vec{y}^{s'}\| = \frac{\sqrt{2}}{2}(1 - z_0^{s'}) \quad (69)$$

and

$$\|\Delta \vec{y}^{s''}\| = \frac{\sqrt{2}}{2}(1 + z_0^{s''}) \quad (70)$$

and obtain

$$z_0^s = \sum_\beta g_\beta^s \frac{1}{\sqrt{2}} \|\vec{w}_\beta^{(2)}\| \cos(\phi_{\Delta y^s} - \phi_\beta) \vec{w}_\beta^{(1)} \vec{x}^s. \quad (71)$$

We assume disjoint effective datasets and one or more neurons 'assigned' to each effective dataset. For each effective dataset, we assume the neurons have the same target direction for their incoming weights:

$$\vec{w}_\beta^{(1)*} = k_\beta \vec{w}_\alpha^{(1)*} \quad (72)$$

with k_β a positive scalar.

Assume the neuron α is aligned to class 1, $\phi_\alpha = \phi_\alpha * 1$. Define:

$$\vec{m}^{/\!/C_1} = \frac{1}{2} \left[\sum_{s'} \vec{x}^{s'} - \sum_{s''} \vec{x}^{s''} \right] \quad (73)$$

and

$$Q^{/\!/C_1} = -\frac{1}{2} \sum_\beta k_\beta \left[\sum_{s' \in C_1} \cos(\phi_{\Delta y^{s'}} - \phi_\beta) \vec{x}^{s'} (\vec{x}^{s'})^T - \sum_{s'' \in C_2} \cos(\phi_{\Delta y^{s''}} - \phi_\beta) \vec{x}^{s''} (\vec{x}^{s''})^T \right] \quad (74)$$

$$= \sum_{\beta \neq C_1} k_\beta \left[\sum_{s' \in C_1} \vec{x}^{s'} (\vec{x}^{s'})^T + \sum_{s'' \in C_2} \vec{x}^{s''} (\vec{x}^{s''})^T \right] - \sum_{\beta \neq C_1} k_\beta \left[\sum_{s' \in C_1} \vec{x}^{s'} (\vec{x}^{s'})^T + \sum_{s'' \in C_2} \vec{x}^{s''} (\vec{x}^{s''})^T \right] \quad (75)$$

$$= \left(\sum_{\beta \neq C_1} k_\beta - \sum_{\beta \neq C_1} k_\beta \right) \left[\sum_{s' \in C_1} \vec{x}^{s'} (\vec{x}^{s'})^T + \sum_{s'' \in C_2} \vec{x}^{s''} (\vec{x}^{s''})^T \right] \quad (76)$$

we then obtain:

$$\vec{\gamma}_\alpha = \vec{m}_0^{/\!/C_1} + Q^{/\!/C_1} \vec{w}_\alpha^{(1)*} = 0 \iff \vec{w}_\alpha^{(1)*} = -\vec{m}^{/\!/C_1} (Q^{/\!/C_1})^{-1} \quad (77)$$

The zeroth order approximation yields $\vec{m}_0^{/\!/C_1}$, and the second order approximation tells us this vector needs to be rotated according to the second order moments of the datasets as given by $Q^{/\!/C_1}$. Higher order approximations will involve higher order moments of the effective datasets.

F. Unlocking

We start from the equations of the gradient of the norms:

$$\left\langle \frac{\partial L^s}{\partial \|\vec{w}_\alpha^{(2)}\|} \right\rangle = -\langle h_\alpha^s \|\vec{y}^s\| \cos(\phi_{\vec{y}^s} - \phi_\alpha) \rangle \quad (78)$$

$$\left\langle \frac{\partial L^s}{\partial \|\vec{w}_\alpha^{(1)}\|} \right\rangle = -\|\vec{w}_\alpha^{(2)}\| \|\vec{\gamma}_\alpha^s\| \cos(\theta_{\langle \vec{\gamma}_\alpha^s \rangle, i} - \theta_{\alpha, i}) \quad (79)$$

with $h_\alpha^s = \vec{w}_\alpha^{(1)} \vec{x}^s + b_\alpha$, and $\vec{\gamma}_\alpha^s$ is given by eq. 67. We will use $b_\alpha \approx 0$, as it starts from $b_\alpha = 0$ at initialization, also only grows significantly when the vector $\vec{w}_\alpha^{(1)}$ is oriented close to its target vector (see eq. 39), but is still orders of magnitude smaller than $\|\vec{w}_\alpha^{(1)}\|$ at that point (depending on the initialization scale of $\vec{w}_\alpha^{(1)}$). Using

$$\langle h_\alpha^s \|\vec{\Delta y}^s\| \cos(\phi_{\vec{\Delta y}^s} - \phi_\alpha) \rangle = \langle (\vec{w}_\alpha^{(1)} \cdot \vec{x}^s) \|\vec{\Delta y}^s\| \cos(\phi_{\vec{\Delta y}^s} - \phi_\alpha) \rangle = \|w_\alpha^{(1)}\| \|\langle \vec{\gamma}_\alpha^s \rangle\| \cos(\delta_\alpha) \quad (80)$$

with $\delta_{\alpha,i}$ be the remaining angular distance, $\delta_{\alpha,i} = \delta_{\alpha,i}(t) = \theta_{\langle \vec{\gamma}_\alpha^s \rangle, i} - \theta_{\alpha,i}$. We thus obtain:

$$\frac{\partial L}{\partial \|\vec{w}_\alpha^{(1)}\|} = -\|w_\alpha^{(2)}\| \|\langle \vec{\gamma}_\alpha^s \rangle\| \cos(\delta_\alpha) \quad (81)$$

$$\frac{\partial L}{\partial \|\vec{w}_\alpha^{(2)}\|} = -\|w_\alpha^{(1)}\| \|\langle \vec{\gamma}_\alpha^s \rangle\| \cos(\delta_\alpha) \quad (82)$$

We first note, as also discussed in (Tarmoun et al., 2021) in a different context, that we can make use of a conserved quantity:

$$\frac{\partial(\|\vec{w}_\alpha^{(2)}\|^2 - \|\vec{w}_\alpha^{(1)}\|^2)}{\partial t} = 2\|\vec{w}_\alpha^{(2)}\| \frac{\partial \|\vec{w}_\alpha^{(2)}\|}{\partial t} - 2\|\vec{w}_\alpha^{(1)}\| \frac{\partial \|\vec{w}_\alpha^{(1)}\|}{\partial t} = 0 \quad (83)$$

which yields:

$$\|\vec{w}_\alpha^{(2)}\|^2 - \|\vec{w}_\alpha^{(1)}\|^2 = c_\alpha \quad (84)$$

with c_α a constant.

Consider the product $a_\alpha = \|\vec{w}_\alpha^{(2)}\| \|\vec{w}_\alpha^{(1)}\|$. We can then obtain:

$$(\|\vec{w}_\alpha^{(2)}\|^2 - \|\vec{w}_\alpha^{(1)}\|^2)^2 = c_\alpha^2 \quad (85)$$

$$= \|\vec{w}_\alpha^{(2)}\|^4 + 2\|\vec{w}_\alpha^{(2)}\|^2 \|\vec{w}_\alpha^{(1)}\|^2 + \|\vec{w}_\alpha^{(1)}\|^4 \quad (86)$$

$$= \|\vec{w}_\alpha^{(2)}\|^4 - 2a_\alpha^2 + \|\vec{w}_\alpha^{(1)}\|^4 \quad (87)$$

$$\iff c_\alpha^2 + 2a_\alpha^2 = \|\vec{w}_\alpha^{(2)}\|^4 + \|\vec{w}_\alpha^{(1)}\|^4 \quad (88)$$

yielding:

$$\frac{\partial a_\alpha}{\partial t} = -\langle \lambda \left(\|\vec{w}_\alpha^{(1)}\| \frac{\partial \|\vec{w}_\alpha^{(2)}\|}{\partial t} + \|\vec{w}_\alpha^{(2)}\| \frac{\partial \|\vec{w}_\alpha^{(1)}\|}{\partial t} \right) \rangle \quad (89)$$

$$= \lambda \|\langle \vec{\gamma}_\alpha^s \rangle\| (\|\vec{w}_\alpha^{(1)}\|^2 + \|\vec{w}_\alpha^{(2)}\|^2) \quad (90)$$

$$= \lambda \|\langle \vec{\gamma}_\alpha^s \rangle\| \cos(\delta_\alpha) \sqrt{c_\alpha^2 + 4a_\alpha^2} \quad (91)$$

As discussed in (Tarmoun et al., 2021), under the assumption of small initial conditions, we can assume $c_\alpha \approx 0$. If we furthermore assume $\vec{w}_\alpha^{(2)}$ is already aligned and we are in the phase of learning where $\|\vec{\Delta y}^s\| \approx \frac{\sqrt{2}}{2}$ for all s in the effective dataset, we have that $\|\langle \vec{\gamma}_\alpha^s \rangle\|$ is a constant (during this phase). Furthermore, in the case of small angular distance, we can assume (due to the direction-norm decoupling) that $\delta_{\alpha,i}(t)$ changes very slowly compared to $a(t)$. This yields:

$$a_\alpha(t) \sim e^{\lambda \|\langle \vec{\gamma}_\alpha^s \rangle\| \cos(\delta_\alpha) t} \quad (92)$$

This represents an exponential growth of $a_\alpha = \|\vec{w}_\alpha^{(2)}\| \|\vec{w}_\alpha^{(1)}\|$ with an exponent determined by $\cos(\delta_\alpha) \leq 1$. Thus neurons that are closer to their target direction grow exponentially faster in norm.

G. Aligned neurons reduce the loss

To show that aligned neurons that grow in norm cause the loss to drop, we show that $\frac{\partial \langle \|\vec{\Delta y}^s\| \rangle}{\partial a_\alpha}$ is negative for an aligned neuron α .

Here $a_\alpha = \|\vec{w}_\alpha^{(2)}\| \|\vec{w}_\alpha^{(1)}\|$.

We have for $\|\Delta y^s\|$ when s is a sample of class 1:

$$\|\Delta y^s\| = \sqrt{(1 - \hat{p}^s)^2 + (0 - (1 - \hat{p}^s))^2} = \sqrt{2}(1 - \hat{p}^s) \quad (93)$$

and for samples of class 2:

$$\|\Delta y^s\| = \sqrt{(0 - \hat{p}^s)^2 + (1 - (1 - \hat{p}^s))^2} = \sqrt{2}\hat{p}^s \quad (94)$$

Thus, we have, for the average over the effective dataset of neuron α :

$$\langle \|\Delta y^s\| \rangle = \frac{N_1^e}{N^e} \langle \|\Delta y^s\| \rangle_{C_1} + \frac{N_2^e}{N^e} \langle \|\Delta y^s\| \rangle_{C_2} \quad (95)$$

$$= \frac{N_1^e}{N^e} \sqrt{2}(1 - \langle \hat{p}^s \rangle_{C_1}) + \frac{N_2^e}{N^e} \sqrt{2}\langle \hat{p}^s \rangle_{C_2} \quad (96)$$

In the regime we are considering, we have $\hat{p}^s \approx \frac{1}{2} + \frac{1}{2}z_0^s$, and

$$z_0^s = \sum_{\beta'//\text{class1}} g_{\beta'}^s w_{\beta',0}^{(2)} \vec{w}_{\beta'}^{(1)} \vec{x}^s + \sum_{\beta''//\text{class2}} g_{\beta''}^s w_{\beta'',0}^{(2)} \vec{w}_{\beta''}^{(1)} \vec{x}^s \quad (97)$$

Here the index β' runs over all neurons aligned to predict class 1 ($\phi_{\beta'} = \phi^{1*}$) and the index β'' runs over all neurons aligned to predict class 2 ($\phi_{\beta'} = \phi^{2*}$). We include the gating vectors of all neurons to indicate if their effective datasets also contains the sample s . I.e., $g_{\beta'}^s = 1$ if the given sample (here an effective sample for neuron α) is also an effective sample for neuron β' , and $g_{\beta'}^s = 0$ otherwise.

Assuming $\alpha//\text{class1}$ (the other case is similar), the contribution of neuron α to z_0^s is given by:

$$\langle z_0^{s,\alpha} \rangle = w_{\alpha,0}^{(2)} \vec{w}_{\alpha'}^{(1)} \langle \vec{x}^s \rangle \quad (98)$$

and for its contribution to $\langle \|\Delta y^s\| \rangle$, we get:

$$\langle \|\Delta y^s\| \rangle^\alpha = \frac{N_1^e}{N^e} \sqrt{2} \left(\frac{1}{2} - \frac{1}{2} \langle z_0^{s,\alpha} \rangle_{C_1} \right) + \frac{N_2^e}{N^e} \sqrt{2} \left(\frac{1}{2} + \frac{1}{2} \langle z_0^{s,\alpha} \rangle_{C_2} \right) \quad (99)$$

$$= c + \frac{\sqrt{2}}{2} w_{\alpha,0}^{(2)} \vec{w}_{\alpha'}^{(1)} \left[-\frac{N_1^e}{N^e} \langle \vec{x}^s \rangle_{C_1} + \frac{N_2^e}{N^e} \langle \vec{x}^s \rangle_{C_2} \right] \quad (100)$$

with c a constant. As $\alpha//\text{class1}$, meaning $\phi_\alpha = \phi^{1*} = \frac{7\pi}{4}$, we have that $w_{\alpha,0}^{(2)} = \frac{\|\vec{w}_\alpha^{(2)}\|}{\sqrt{2}}$. Moreover, when aligned and in the early phase of training, we know the direction of $\vec{w}_\alpha^{(1)}$ is close to the direction of $\vec{m}^1 = +\frac{N_1^e}{N^e} \langle \vec{x}^s \rangle_{C_1} - \frac{N_2^e}{N^e} \langle \vec{x}^s \rangle_{C_2}$, which is the opposite direction to the vector in the equation above. We thus obtain:

$$\frac{\partial \langle \|\Delta y^s\| \rangle}{\partial a_\alpha} = \frac{\partial}{\partial a_\alpha} \left[\frac{1}{2} \|\vec{w}_\alpha^{(2)}\| \|\vec{w}_\alpha^{(1)}\| \|\vec{m}^1\| \cos(\pi + \Delta) \right] \quad (101)$$

$$= \frac{1}{2} \|\vec{m}^1\| \cos(\pi + \Delta) \quad (102)$$

with Δ the angular distance between \vec{m}^1 and $\vec{w}_\alpha^{(1)}$, a small angle. The sign of the derivative is thus negative.